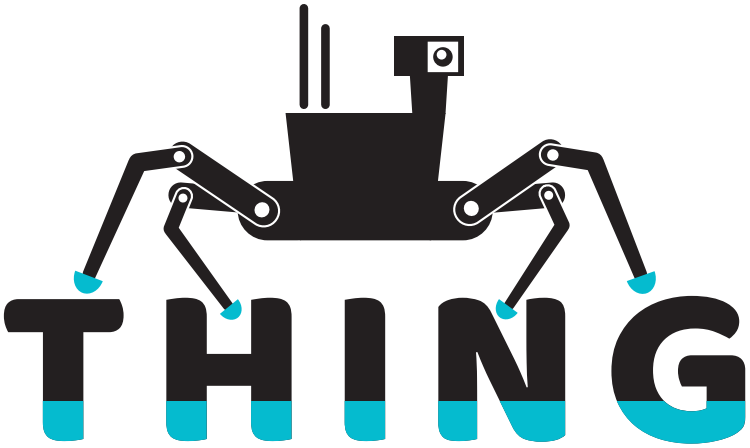

subTerranean Haptic INvestiGator

H2020-ICT-2017-1
Grant agreement no: 780883

DELIVERABLE 3.3

Technical report describing the performance of friction and vibration sensing

Due date: month 45 (September)
Deliverable type: R
Lead beneficiary: PUT

Dissemination Level: PUBLIC

Main author: Krzysztof Walas

Contents

List of Figures

1 Introduction

This technical report describes the progress made in the THING project towards the analysis of terrain friction on the ANYmal robot and towards vibration sensing capabilities via sole in the underground mine. The document is divided into two sections. First, the friction analysis will be described then we will move on to vibration sensing.

2 Friction sensing

2.1 Background

In legged robotics, the information on physical parameters of the terrain the robot is traversing is crucial to perform efficient walking, i.e., by gait adaptation. The physical properties of the terrain might be estimated on the robot implicitly or explicitly. In the first case, one can use the machine learning approach to perform end-to-end learning to map the terrain sensing measurements into actions [14]. The second approach aims to identify the physical parameters of the ground and then provide them to the robot's control system [3]. Our study focused on the latter approach as it allows us to explain the robot behavior during the mission as the physical parameters of the ground are intuitively readable to the human and not hidden in the neural network's weights as in the end-to-end approach. We chose this approach as the industry prefers explainable solutions to black-box ones, and one of the goals of the THING project was to show the industrial viability of the subterranean haptic investigator.

The most affordable and the most common sensor in mobile robotics is an RGB camera. The prediction of the terrain friction from vision for the control of the humanoid robot walk was described in [4]. However, the main drawback of RGB-only approaches is the poor performance in material classification and parameter estimation tasks due to various visual artifacts [9]. To improve the classification of materials, authors of [8] used spectral analysis, while Saponaro et al. [19] incorporated knowledge about water permeation and its cooling/heating cycle. Another approach uses reflectance images [23].

The other way of getting an additional source of information for friction estimation is to push the objects and observe their interaction with the environment [15]. There are also approaches to friction estimation without a need to visually inspect the scene and measure reaction forces during the interaction with the materials as with the exploratory moves proposed in [12] and in [13]. Moreover, Ridgewell et al. [18] performed online friction estimation for contact exploitation in a simulated biped robot control. However, it was done only for a single value of friction coefficient in a single experiment. The more extensive research was presented in [3].

2.2 Materials and Methods

For the test of our approach, we used PUTANY dataset that was introduced in [5]. The data was gathered with ANYmal B300 robot continuously walking on eight different real-world terrain samples with no additional exploratory moves. The quadrupedal walking robot was equipped with four compliant and sensorized feet (presented in Fig. 1), providing force and torque signals during the dataset acquisition.

The experiments were performed on eight terrain types (carpet, artificial grass, rubber, sand, foam, rocks, ceramic tiles, PVC tiles) that were arranged to form a

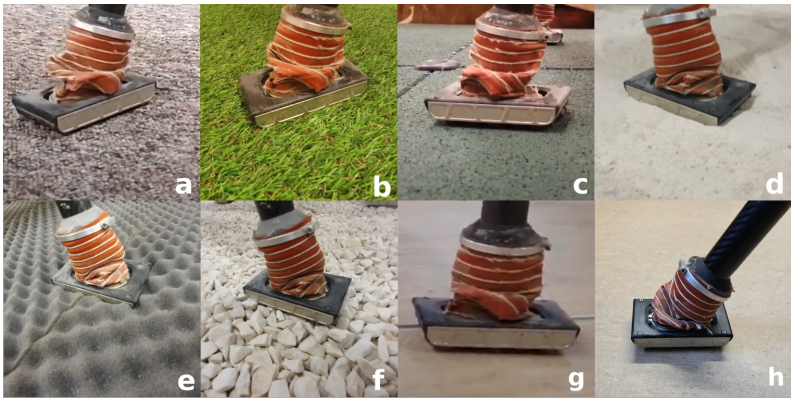

Figure 1: Sensorized feet on different terrain types included in the dataset: *carpet* (a), *artificial grass* (b), *rubber* (c), *sand* (d), *foam* (e), *rocks* (f), *ceramic tiles* (g), *PVC* (h).

continuous walking area. The walking area contained two steep ramps, which can be seen in Fig. 2. For each step stored in the PUTANY dataset, we know the semantic terrain class and force/torque signals measured at the feet, as the external ground truth Optitrack system was used to know the accurate location of the robot.

Figure 2: The ANYmal robot walking over the prepared terrain course to collect dataset.

We started by analytically estimating the static friction coefficient μ of all the terrains used in the ANYmal experiment to make the friction identification process possible. We did this using the test bench with the robotic manipulator operating in the controlled force mode. The test bench consisted of a Universal Robots UR3 robotic arm and Rokubimini sensorized feet, as shown in Figure 3. The used feet are the same as the one used on ANYmal robot when gathering PUTANY dataset.

To learn the friction coefficient μ, we had to apply the F_n along the gravity vector and apply linearly increasing F_f perpendicular to the normal. The time instance when a leg moves indicate the necessary force F_f^* needed to move a leg on a selected terrain type. The static friction coefficient μ can be computed based on the equation:

$$\mu = \frac{F_f^*}{F_n}. \tag{1}$$

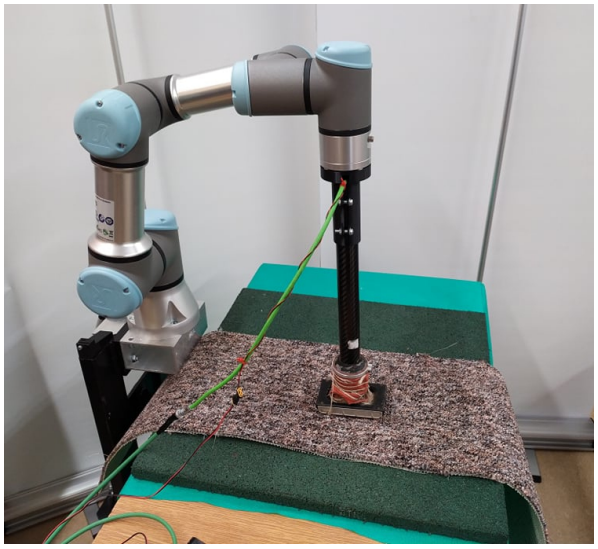

Figure 3: Setup used to collect a friction force dataset, consisting of Universal Robots UR3 robotic arm with Rokubimini sensorized foot. The robot was programmed to perform a sampling action, moving a foot in X-axis while applying force in Z-axis.

The forces must be applied in accurate directions during these experiments, which was guaranteed with the industrial robotic arm.

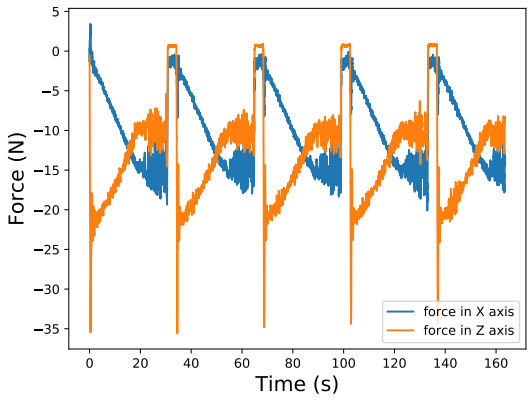

Figure 4: Sample of dataset recorded on artificial grass terrain type. The force measurements were recorded with frequency equals 200 Hz. The robot's move was performed in 'force mode'.

In our experiments, we gathered the force/torque measurements with 200 Hz, as shown in Figure 4. To determine the friction component μ, we need to determine the instance of a time, called point of interest, when the feet are no longer static from the registered force/torque signals, and we can calculate the based on force reading. To determine the point of interest, we follow the algorithm:

1. Smooth signal of force with moving average window of 100 samples (approx. 0.5

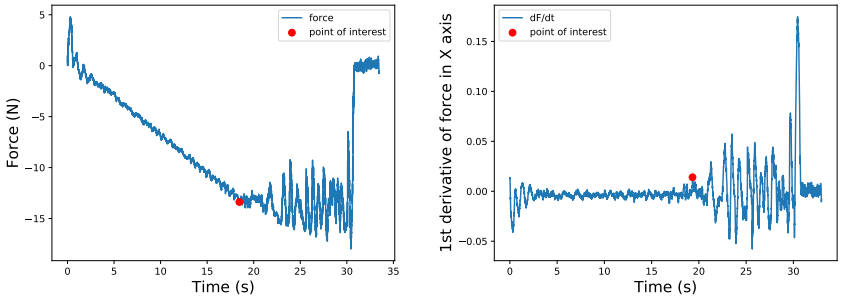

Figure 5: (a) Force in X-axis (b) 1st derivative of force in X-axis

Terrain	Friction coeff. (mean)	Friction coeff. (std. dev.)
Art. grass	1.52	0.11
Carpet	1.99	0.12
Ceramic Tiles	0.58	0.02
Foam	1.59	0.20
Rubber	1.36	0.05
PVC	0.81	0.07
Rocks	0.69	0.19
Sand	0.53	0.02

Table 1: Results of force signal analysis. Friction coefficient calculated as a mean of 10 sampling moves.

seconds).

2. Calculate the gradient of force over time to get a signal presented in Fig. 5b.
3. Localize point of interest based on a change in gradient.
4. Take 20 samples of force measurements along the gravity vector and perpendicular to the normal prior to the point of interest.
5. Calculate mean forces from these 20 samples.
6. Calculate friction coefficient using eq. 1.

The values of a mean and a standard deviation of friction coefficient obtained for different materials are presented in Table 1. For every material, there were ten robot sampling moves performed.

For a couple of materials (artificial grass, carpet, foam, rubber), the μ value exceeds 1. This situation is caused by the shape of the sole of the robot foot, which has tabs and for certain materials is causing the hooking in the terrain samples for specific materials.

2.3 Proposed approach

In our research, we propose to perform friction coefficient regression using a neural network. We have experimented with the size of the layers and finally found that the architecture with successive layers: Fully Connected (FC) -> Batch Normalization

-> Rectified Linear Unit (ReLU) -> Dropout(0.2)-> Fully Connected (FC) on top of the previously introduced encoder as a regression head is providing us with the best estimate of friction coefficients. The architecture of the proposed neural network is shown in Figure 6. The architecture was inspired by our previous network used for efficient terrain classification in localization tasks [5]. In the current implementation, latent vector size is equal to 128. We used the loss function Mean Absolute Error (MAE), which computes arithmetic average of the absolute errors between the predicted and estimated friction coefficients. We used AdamW optimizer with a learning rate of 0.001 with exponential decay.

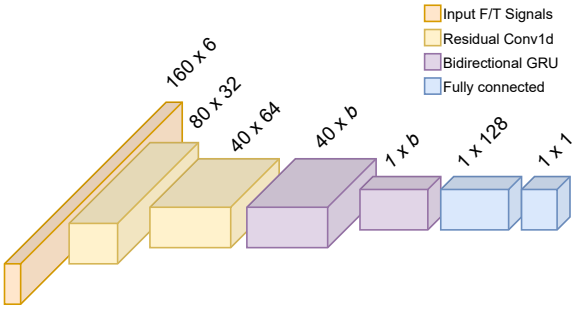

Figure 6: Neural network used in friction coefficient regression. FC->BatchNorm->ReLU->Dropout(0.2)->FC at the end as a regression head. Standarization and encoder same as in [5] with latent vector size $b = 128$. Loss function: MAE, optimizer: AdamW, learning rate weight: 0.001 with exponential decay.

2.4 Results

We have performed two types of experiments. In the first one, we enriched a PUTANY dataset with friction coefficients for every terrain type estimated from the testbed with the robotic arm. Then, all the data for each friction coefficient was randomly divided into 3443 learning samples, 1148 evaluation samples, and 1148 test samples. After 350 epochs, the network reached the test set's loss value $MAE = 0.0606$ (Figure 7). We also checked other parameters of learning in the task of regression. Mean absolute percentage error $MAPE = 5.4335$ (Figure 8) and mean squared error $MSE = 0.0202$ (Figure 9).

In Table ,2 we presented predicted values of friction coefficients using the proposed neural network on the test set of the PUTANY dataset.

To test the generalization capabilities of our approach to friction coefficient estimation, we performed tests using cross-validation and excluded samples for artificial grass and foam from learning data and then tested samples for these terrains. This simulated the performance of friction estimation on previously unseen terrain. For artificial grass ($\mu = 1.52$) and foam ($\mu = 1.59$) excluded from the learning dataset the numerical results on test set after 250 epochs are $MAE = 0.4357$ and $MAPE = 29.5589$. The learning evaluation and testing process is shown in Figure 10 and Figure 11. The obtained errors are significant but show that the method can generalize well to the previously unseen terrains.

When we exclude two different materials of rubber ($\mu = 1.36$) and carpet ($\mu = 1.99$) from learning, the numerical results on the test set after 250 epochs for these materials are $MAE = 0.3429$ and $MAPE = 20.0412$. The learning evaluation and testing

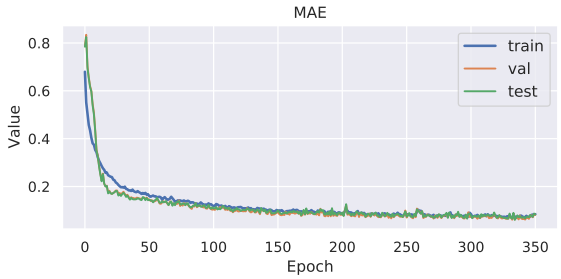

Figure 7: Loss function on train, validation and test sets. Final value on test set = 0.0606

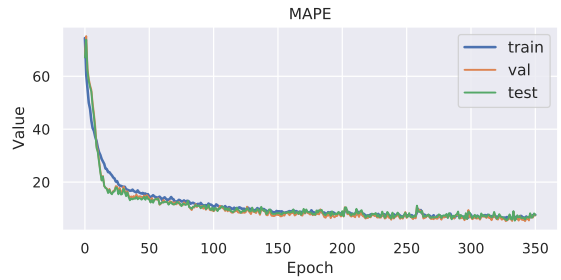

Figure 8: MAPE on train, validation, and test sets. Final value on test set = 5.4335

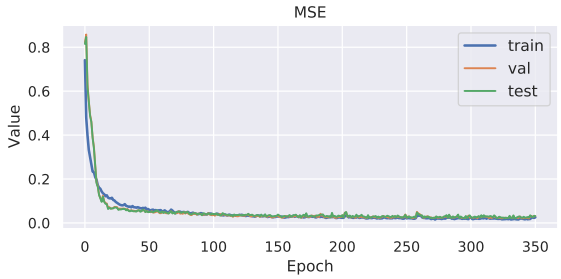

Figure 9: MSE on train, validation and test sets. Final value on test set = 0.0202

process is shown in Figure 12 and Figure 13.

The results for learning on the whole set where the data for each friction coefficient was used have Mean Absolute Percentage Error equal to 5.4335, which provide us with the measure of prediction accuracy. For the legged robotic tasks, the prediction of friction coefficient with the error of approximately 5% and providing it to the dynamics model will improve the robot's mobility. Currently, the dynamics of the contacts are set to some conservative values so the robot can cope with the majority of the encountered terrain. In situations when our robot didn't have all the terrain parameters in the learning set, which is the case in real-world scenarios, we need to rely on the generalization property of the network. In our case, such generalization

Terrain	Ground truth	Frict. coeff. (mean)	Differ. [%]	Std. dev.
Art. grass	1.52	1.45	4.61	0.27
Carpet	1.99	1.9	4.52	0.18
Ceramics	0.58	0.6	3.45	0.12
Foam	1.59	1.52	4.4	0.13
Rubber	1.36	1.38	1.47	0.08
PVC	0.81	0.84	3.7	0.16
Rocks	0.69	0.69	0.0	0.09
Sand	0.53	0.56	5.66	0.05

Table 2: Results of predicting friction coefficients for different terrains using neural network.

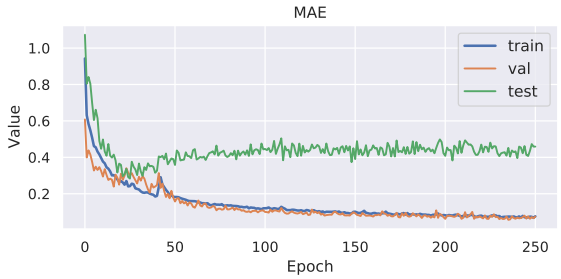

Figure 10: Loss function with grass and foam in the test set.

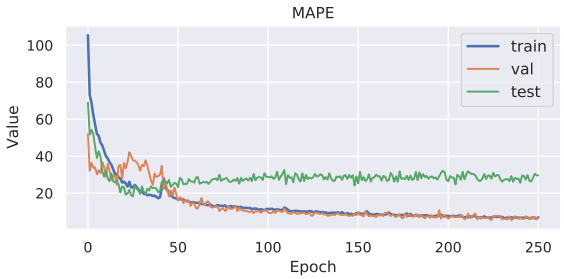

Figure 11: MAPE on grass and foam in the test set.

provided us with a MAPE of approximately 20% to 30% depending on how far our testing data was from the search space used in the learning part. These values are still acceptable, considering the current approach with the constant value used in the contact dynamics model regardless of the terrain.

3 Vibration sensing

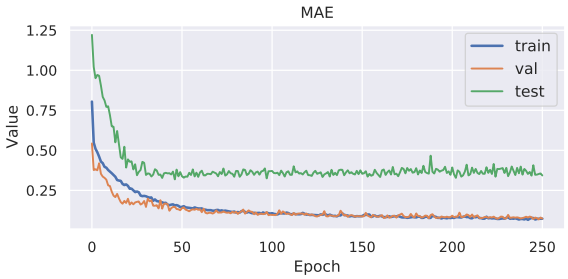

Figure 12: Loss function on rubber and carpet in the test set.

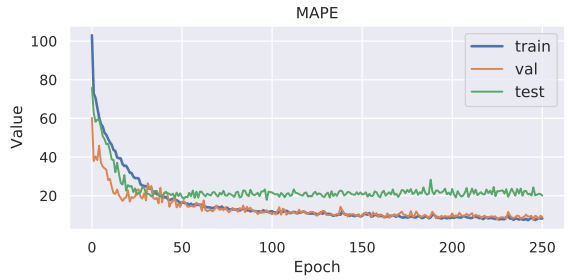

Figure 13: MAPE on rubber and carpet in the test set.

3.1 Background

Vibration is one of the most frequently used and best-researched signals utilized to assess the "health" of a machine and its correctness of operation. The vibration signal is collected using a three-axis accelerometer, often part of the IMU sensor (inertial measurement unit). The measurement itself can be performed in several ways, including magnetic sensor mounting, adhesive mounting, thread mounting, etc. In industrial solutions, two types of vibration data collection can be distinguished most often. The first of them are sensors mounted "permanently" with glue or a special mounting point. This configuration is costly as each measured item must be fitted with a sensor and connected to the network but allows for real-time data analysis and accurate predictions. The opposite of this method is an inspection where qualified personnel collect data from machines with a vibrometer and either analyze it immediately or submit it for later analysis. This method is relatively cheaper and widely used since mechanical machines usually give premises (signal anomalies) much earlier before failure.

On the other hand, vibration analysis is mainly done in the frequency or Falk domain, although there are time-domain approaches to the topic such as [7, 10, 6]. On the other hand, the frequency domain is most effective if the analyzed machine has rotational elements. There are numerous techniques of machine condition monitoring using vibration frequency analysis like higher-order techniques [11], connection with wavelet techniques [1], nonstationary techniques [17], statistical analysis [21], periodic autoregressive spectral estimator [20], Hilbert-Huang transform [22], and many others [16].

Sensor	Period [s]	Frequency [Hz]
Stiff Leg	0.004892	204.429759
Adaptive Leg	0.005402	185.117255
Accelerometer	0.004890	204.513931

The saptionSampling frequency of sensors

3.2 Proposed approach

In the course of the project, experiments were carried out consisting in measuring vibrations with the help of an ANYmal robot sensory limb. The experiments were carried out at the Ore Enrichment Plant of KGHM Polska Miedź SA, located in Polkowice, Poland. The experiments aimed to evaluate the quality of the measurement with the sensory limb in relation to the currently used measurement methods. The experiments consisted in taking one-minute measurements of the belt conveyor drive vibrations with three states of the limbs (stiff limb, adaptive limb, magnetically mounted accelerometer) at 3 points (A - front of the gearbox housing, B - top of the gearbox housing, C - top of the connection between gearbox and flexible coupling). The experiment was repeated on 4 conveyor drives, which gave a total of 36 one-minute samples (two of which failed). The points are shown in Fig. 14, while Fig. 15 shows the graphs of the raw signals.

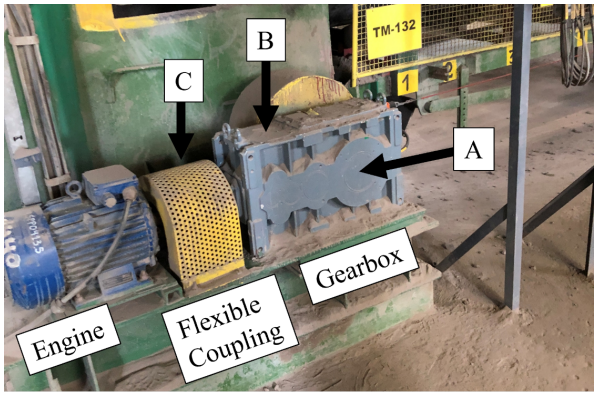

Figure 14: Conveyor drive with marked measurement points: A - front of gearbox casing, B - top of gearbox casing, C - top of a flexible coupling.

3.3 Results

Initially, it was decided to analyze the samples in terms of constancy in sampling and maintaining the assumed sampling frequency. The analysis consisted in calculating the average period between the samples, converting it to frequency, and comparing it with the assumed frequency. The analysis results are shown in Table ??, from which it is clear that the stiff leg and the accelerometer sensor maintained a similar sampling rate of 204.5 Hz, while the adaptive leg decreased to about 185 Hz.

After the sampling analysis, it was decided to examine the sensors in terms of their primary task, i.e., frequency analysis (as most algorithms are based on the frequency domain of vibrations). To this end, each of the 36 signals was subjected to a Fast Fourier Transform (FFT). The Fourier transform decomposes the base signal into frequency components, thus causing its transition from the time domain to the

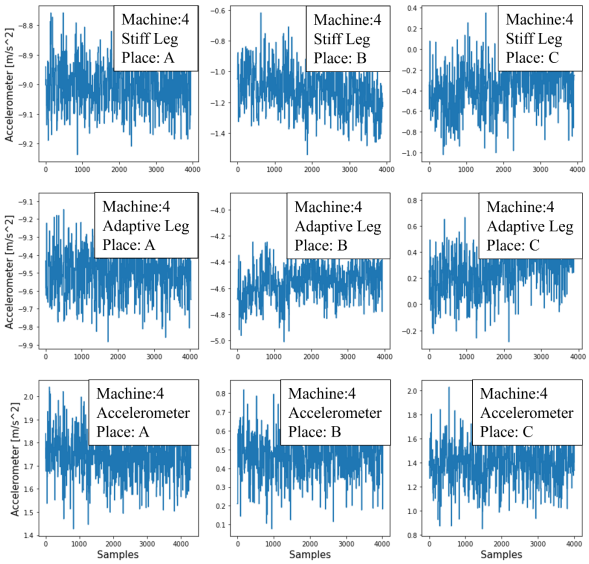

Figure 15: Raw data collected from one machine by 3 sensors in 3 different measurement points

frequency domain. Amplitude spectra calculated from samples and their filtered version (moving average filter - red color) are presented in Fig. 16. What can be observed is a single peak visible in some graphs, being around 11 - 12 Hz, which gives 660-720 RPM. After consultation with the operators, it was found that this is the standard rotational speed for the tested types of conveyors, taking into account their work.

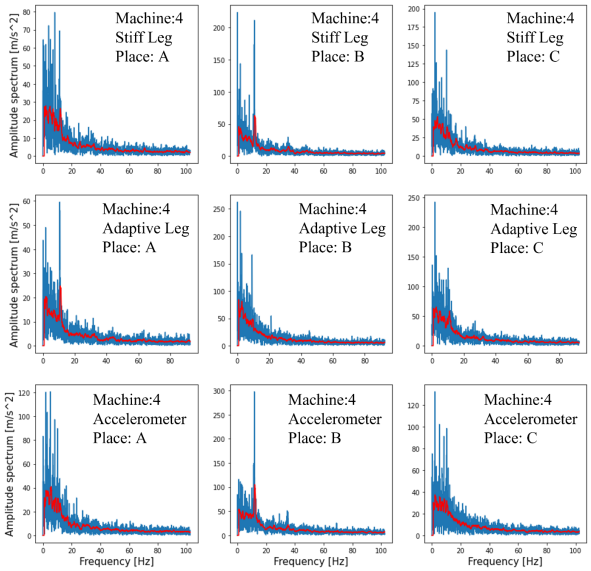

Figure 16: Frequency spectrum from signal taken from machine 4

Conveyor drive	Sensor	Frequency in place A [Hz]	Frequency in place B [Hz]	Frequency in place C [Hz]
A	Stiff Leg	11.22	11.16	12.04
	Adaptive Leg	11.13	11.18	11.10
	Accelerometer	11.03	damaged	11.14
B	Stiff Leg	11.16		10.45
	Adaptive Leg	11.31		11.46
	Accelerometer	12.15	11.42	11.21
C	Stiff Leg	12.35	12.30	12.40
	Adaptive Leg	11.13		damaged
	Accelerometer	12.23	12.33	11.32
D	Stiff Leg	12.31	12.18	12.03
	Adaptive Leg	12.23	12.33	12.31
	Accelerometer	10.35	10.44	10.24

Table 3: Occurrence of the main frequency component denoting work.

After determining the frequency of regular operation of the conveyor, it was decided to test its presence in other signals from the sensors. The results of this study are shown in Table 3. It shows that the operating frequency of the drive fluctuates in the range of 10-12 Hz depending on the machine, measuring place, and sensor used.

3.4 Application of the diagnostic procedure for conveyor gears

In the case of a conveyor, vibration measurements using the haptic leg are possible to apply in diagnostics of rotational elements of gearboxes. Gearboxes are one of the critical elements of the conveying system. In terms of developing the methodology for diagnosing the gears, it was necessary to obtain:

1. procedure for measuring vibrations performed by a robot.
2. procedure for the calculation of diagnostic features ensuring the detection of damage to shafts, gears, and rolling bearings.
3. procedure for identifying threshold values for measured characteristics for decision making.

3.4.1 Procedure for measuring vibrations performed by a robot (diagnostic mission)

The main goal of the THING project was to adapt the robot to the inspection tasks of the conveyor transport infrastructure in mining application as well as the inspection of the excavation itself. Inspection task scenarios are summarized in detail in [7]. The robot must be able to completely reproduce typical inspection tasks performed by a maintenance employee using advanced sensors and algorithms for diagnostic inspection of the conveyor drive unit gearbox. The main challenge is the complete elimination of the human role in the evaluation of the technical condition of the gearbox. We eliminate both human exposure to the risk of working in danger and erroneous technical condition assessments, which are often made using human senses (subjective impressions). The measurement procedure depicted in the Figure below indicates the measurement points. This measurement method does not require assembling sensors to the drive unit. The measurement is performed with haptic sensing.

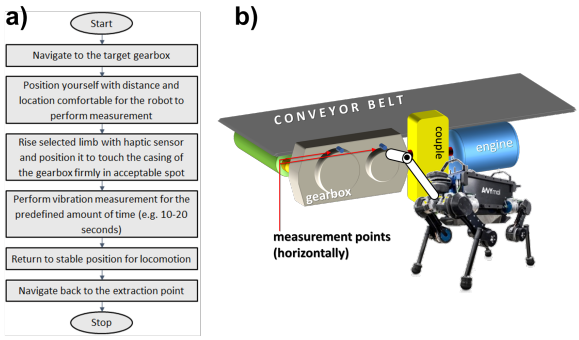

Figure 17: Procedure of inspection mission with ANYmal robot for belt conveyor gearbox, b) measurement points

3.4.2 Procedure for the calculation of diagnostic features ensuring the detection of damage to shafts, gears, and rolling bearings

Diagnostic features of multistage gearboxes can be identified by transforming the signal into the frequency domain and further defining components relative to the specific vibration elements (shafts, gearing, bearings) in its spectrum. Thus, the comprehensive condition of the components of the gearbox under inspection might be obtained. To obtain a universally applicable method to all mine conveyors, assumptions dedicated to mining conveyors proposed by Prof. Bartelmus have been used[2]. The diagnostic features extraction method used is a modifying method proposed by Bartelmus and employs the broadband Fourier transform to translate the signal into the frequency domain. The methodology adopted the vibration measurement for the 20s. Next, the raw signal was evenly segmented into 20 sections. Repetitively, each consecutive 1-second section of vibration signal was converted into the frequency domain. All obtained sections were totaled within three spectrum frequency bands (for shafts: 10-100 Hz, for gears: 100-3500 Hz, for bearings: 3500-10000 Hz). The measurement results in 20-second time series (with a sample period of 1s) of diagnostic features sDF (shafts diagnostic feature), gDF (gearbox diagnostic feature), and bDF (bearings diagnostic feature), which define the condition of, respectively, shafts, gears, and bearings.

3.4.3 Procedure for identifying threshold values for measured characteristics for decision making

The development of decision thresholds necessitates the acquisition of an extensive diagnostic database. It is crucial to have measurements of diagnostic features from healthy and unhealthy objects. The threshold values must be defined separately for each gear type. Users can empirically determine them for diagnostic features, separately for shafts, gears, and bearings. As the diagnostic base grows, the user will be able to learn about the evolution of failures and their different stages, and finally, adjust the threshold values more. The diagnostic features acquired during the project were analyzed. The analyzes show that the data have a Weibull distribution, and the estimation of the parameters of this distribution gives a better insight into the estimation of the residual lifetime of the gearbox.

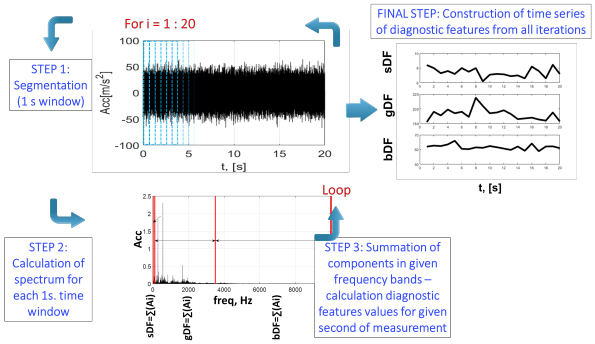

Figure 18: The methodology of identifying diagnostic features from vibration signal spectrum

4 Conclusion

In the current technical report, the friction analysis for the legged robots was presented. The obtained results show that the accuracy of the estimated friction coefficient is suitable for the purposes of legged locomotion. We tested that in two scenarios. When where the robot has the complete learning set and in the case encountered in a reality where the robot encounters the ground substrates absent in the learning set.

In the vibration part of the report, the analyses found that both investigated alternatives to a magnetically mounted accelerometer provide similar accuracy in the vibration measurement. The stiff leg was slightly better because it offered a sampling rate identical to an accelerometer. As a result, it is a recommended tool for measurement. In addition, frequency-domain vibration analyzes showed that all three limbs were able to register, to a varying degree, the native frequency of the conveyor belt drive. This allows you to determine the health and correctness of the machine's operation by tracking this and other dominant frequencies.

References

[1] Fadi Al-Badour, Mehmet Sunar, and Lahouari Cheded. "Vibration analysis of rotating machinery using time-frequency analysis and wavelet techniques". In: *Mechanical Systems and Signal Processing* 25 (2011), pp. 2083–2101.

[2] W. Bartelmus. *Condition monitoring of open cast mining machinery*. Oficyna Wydawnicza Politechniki Wrocławskiej, 2006. ISBN: 9788370859619. URL: https://books.google.pl/books?id=1fWRGQAACAAJ.

[3] W. Bosworth et al. "Robot locomotion on hard and soft ground: Measuring stability and ground properties in-situ". In: *2016 IEEE Int. Conf. on Robotics and Automation (ICRA)*. 2016, pp. 3582–3589. DOI: 10.1109/ICRA.2016.7487541.

[4] M. Brandão et al. "Material recognition CNNs and hierarchical planning for biped robot locomotion on slippery terrain". In: *2016 IEEE-RAS 16th Int. Conf. on Humanoid Robots (Humanoids)*. 2016, pp. 81–88. DOI: 10.1109/HUMANOIDS.2016.7803258.

[5] Russell Buchanan et al. "Navigating by touch: haptic Monte Carlo localization via geometric sensing and terrain classification". In: *Autonomous Robots* (2021). DOI: 10.1007/s10514-021-10013-w.

[6] Tahsin Doguer and Jens Strackeljan. "Vibration Analysis using Time Domain Methods for the Detection of small Roller Bearing Defects". In: (Mar. 2009), pp. 23–25.

[7] Stephan Ebersbach and Zhongxiao Peng. "Expert system development for vibration analysis in machine condition monitoring". In: *Expert Systems with Applications* 34 (Jan. 2008), pp. 291–299. DOI: 10.1016/j.eswa.2006.09.029.

[8] Zackory Erickson et al. "Classification of Household Materials via Spectroscopy". In: (2018). URL: http://arxiv.org/abs/1805.04051.

[9] Roland W. Fleming. "Visual perception of materials and their properties". In: *Vision Research* 94 (2014), pp. 62 –75. ISSN: 0042-6989. DOI: https://doi.org/10.1016/j.visres.2013.11.004. URL: http://www.sciencedirect.com/science/article/pii/S0042698913002782.

[10] Juraj Gerlici and Tomáš Lack. "Modified HHT Method for Vehicle Vibration Analysis in Time Domain Utilisation". In: *Applied Mechanics and Materials* 486 (Dec. 2013), pp. 396–405. DOI: 10.4028/www.scientific.net/AMM.486.396.

[11] I M Howard. "Higher-order spectral techniques for machine vibration condition monitoring". In: *Proceedings of the Institution of Mechanical Engineers, Part G: Journal of Aerospace Engineering* 211.4 (1997), pp. 211–219. DOI: 10.1243/0954410971532622. eprint: https://doi.org/10.1243/0954410971532622. URL: https://doi.org/10.1243/0954410971532622.

[12] Mengqi Ji et al. "Preprocessing-free surface material classification using convolutional neural networks pretrained by sparse Autoencoder". In: *IEEE Int. Workshop on Machine Learning for Signal Processing, MLSP* (2015). ISSN: 21610371. DOI: 10.1109/MLSP.2015.7324324.

[13] Matthias Kerzel et al. "Haptic material classification with a multi-channel neural network". In: *Proc. of the Int. Joint Conf. on Neural Networks* 2017-May (2017), pp. 439–446. DOI: 10.1109/IJCNN.2017.7965887.

[14] Joonho Lee et al. "Learning quadrupedal locomotion over challenging terrain". In: *Science Robotics* 5.47 (2020). DOI: 10.1126/scirobotics.abc5986.

[15] K. M. Lynch. "Estimating the friction parameters of pushed objects". In: *Proceedings of 1993 IEEE/RSJ Int. Conf. on Intelligent Robots and Systems (IROS '93)*. Vol. 1. 1993, 186–193 vol.1. DOI: 10.1109/IROS.1993.583097.

[16] Asoke Nandi and Hosameldin Ahmed. *Condition Monitoring with Vibration Signals: Compressive Sampling and Learning Algorithms for Rotating Machine*. Dec. 2019. ISBN: 9781119544623. DOI: 10.1002/9781119544678.

[17] M.-C. Pan, P. Sas, and H. van Brussel. "Nonstationary time-frequency analysis for machine condition monitoring". In: *Proceedings of Third International Symposium on Time-Frequency and Time-Scale Analysis (TFTS-96)*. 1996, pp. 477–480. DOI: 10.1109/TFSA.1996.550096.

[18] Cameron P Ridgewell et al. "Online estimation of friction constraints for multi-contact whole body control". In: *2017 IEEE-RAS 17th Int. Conf. on Humanoid Robotics (Humanoids)*. IEEE. 2017, pp. 347–352.

[19] Philip Saponaro et al. "Material classification with thermal imagery". In: *Proceedings of the IEEE Computer Society Conf. on Computer Vision and Pattern Recognition* 07-12-June (2015), pp. 4649–4656. ISSN: 10636919. DOI: 10.1109/CVPR.2015.7299096.

[20] J.M. Spanjaard et al. "Periodic autoregressive time-frequency analysis for monitoring of rotating machinery with variable period". In: *Proceedings of Third International Symposium on Time-Frequency and Time-Scale Analysis (TFTS-96)*. 1996, pp. 465–468. DOI: 10.1109/TFSA.1996.550093.

[21] Teng Wang, Guoliang Lu, and Peng Yan. "A Novel Statistical Time-Frequency Analysis for Rotating Machine Condition Monitoring". In: *IEEE Transactions on Industrial Electronics* 67.1 (2020), pp. 531–541. DOI: 10.1109/TIE.2019.2896109.

[22] Ling Xiang, Guiji Tang, and Yongli Zhu. "Vibration Signal Analysis of Rotor System Based on Time-Frequency Attributes". In: *2008 The 9th International Conference for Young Computer Scientists*. 2008, pp. 2713–2717. DOI: 10.1109/ICYCS.2008.171.

[23] Hang Zhang, Kristin Dana, and Ko Nishino. "Friction from Reflectance: Deep Reflectance Codes for Predicting Physical Surface Properties from One-Shot In-Field Reflectance". In: *Computer Vision – ECCV 2016*. Ed. by Bastian Leibe et al. Cham: Springer Int. Publishing, 2016, pp. 808–824. ISBN: 978-3-319-46493-0.